Ultrafast time-gated approach in optical biomedical imaging

B. B. Das and R. R. Alfano*

Institute for Ultrafast Spectroscopy and Lasers, New York State Center for Advanced Technology for Ultrafast Photonic Materials and Applications, Department of Physics, The City College of the City University of New York, 138th Street at Convent Avenue, New York NY 10031, USA

Noninvasive biomedical imaging based on ultrafast photonic methods are being actively pursued by a number of groups. Several time-domain approaches for bone and thick tissue imaging based on streak camera, Kerr–Fourier gate and electronic time-gated imaging techniques are discussed in this paper.

IMAGING an object located in a highly scattering medium is a challenging problem with a wide range of applications in different fields: medicine, industry, defence and space. A better understanding of photon migration in turbid media has resulted in a surge of research interest in optical biomedical imaging. Limitations of X-ray imaging in detecting small lesions in tissues, in distinguishing malignant tumors from benign ones, and the concern regarding potentially harmful effects of ionizing radiation have led to a renewed interest in the development of non-invasive and non-ionizing optical diagnostic and imaging methods[1–32] since the early 1980s. Advances in ultrashort light pulse generation and high-speed optical detection systems have provided the technological support for the development of various optical imaging modalities. A number of different experimental schemes based on cw, time-resolved, and frequency-domain methods, as well as space gating, and polarization gating have evolved over the years for selectively choosing different components of scattered light (ballistic, snake or diffuse) for imaging in a highly scattering medium.

In this paper we briefly describe photon migration in a highly scattering random medium in the diffusion approximation. We illustrate some of the time-resolved imaging modalities – streak camera, Kerr–Fourier imaging and picosecond electronic time-gated imaging – developed at the Institute for Ultrafast Spectroscopy and Lasers, City College of the City University of New York, for biomedical optical imaging.

Photon migration in a turbid medium: Ballistic, snake and diffuse light

Light transport in various random media such as tissues can be quantitatively characterized by a few key optical parameters[33,34]: the scattering coefficient ($\mu_s = n\sigma_s$), the absorption coefficient ($\mu_a = n'\sigma_a$), the total extinction (or attenuation) coefficient (μ_T), and the mean cosine of the scattering angle (g), where n, n', σ_s, and σ_a are the scatterer density, absorber density, single particle scattering cross-section and single particle absorption cross-section, respectively. The absorption length ($l_a = 1/\mu_a$) is the mean distance a photon travels in the medium before it is absorbed. The scattering mean free path ($l_s = 1/\mu_s$) is the mean distance between scattering. The anisotropy of scattering is described through the factor g. The transport mean free path (l_t) is given as: $l_t = 1/n\sigma_m = l_s/(1-g)$, where σ_m is the momentum exchange scattering cross-section of the scatterer. Transport length describes an average of propagation. For small particles $l_s \sim l_t$, while for large particles $l_t \gg l_s$. The total extinction coefficient is given by the sum of the scattering and the absorption coefficients ($\mu_T = \mu_s + \mu_a$).

When an ultrashort laser pulse is incident on a turbid medium, multiple scattering due to random fluctuations in the refractive indices spreads the incident pulse temporally into a coherent (ballistic) component (I_c) and a diffuse component (I_d) (refs 33–35) as shown in Figure 1.

The ballistic part consists of the photons that travel undeviated in the forward direction while the diffuse component consists of the multiple scattered photons. The ballistic component which arises from coherent interference of scattered light in the forward direction is

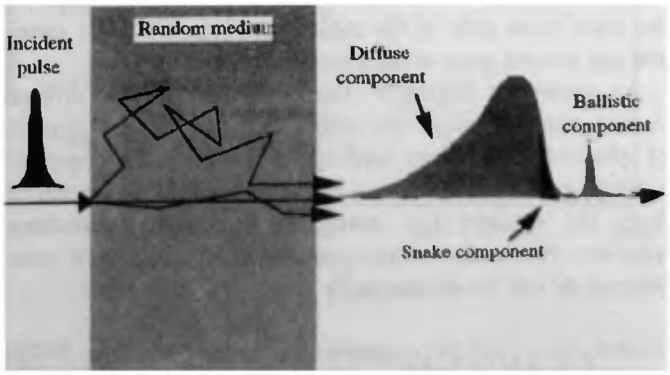

Figure 1. An ultrashort laser pulse propagating through a random medium spreads into a *ballistic*, *snake* and a *diffuse* component. The ballistic photons travel along the straight line path, the diffuse photons undergo random walks and the snake photons traverse zig zag paths slightly off the straight line path through the medium (after ref. 5).

*For correspondence. (e-mail: barikul@scisun.sci.ccny.cuny.edu)

attenuated with the distance of propagation d in the medium as:

$$I_c = I_0 e^{-\mu_T d} \quad (1)$$

where I_0, and μ_T are the incident intensity and the total extinction coefficient ($\mu_s + \mu_a$), respectively. This coherent component, though most desirable for optical imaging, is extremely difficult to detect because of the strong attenuation. That leaves us with the scattered photons forming the diffuse component.

Photon migration in a random medium is generally described by the Transport Theory[33,36]. The difficulty in finding analytical solutions to the transport equation in many cases has led to several approximations, of which diffusion approximation is the most commonly used theory in thick-tissue optics (thickness $> 7l_t$). When the diffuse intensity is expanded in a series of spherical harmonics and only the first two terms are taken, that gives the diffusion approximation[5,34]:

$$I_d(\bar{r}, \hat{n}, t) \approx \phi(\bar{r}, t) + \frac{3}{4\pi} \bar{j}(\bar{r}, t) \cdot \hat{n}, \quad (2)$$

where $\phi(\bar{r}, t) = vn(\bar{r}, t)$. And v and n are the velocity of light and the photon density in the medium respectively and $\bar{j}(\bar{r}, t) = -D\hat{n} \cdot \bar{\nabla} n(\bar{r}, t)$, with the diffusion constant D given as

$$D = \frac{v}{3\{\mu_a + (1-g)\mu_s\}} \approx \frac{vl_t}{3}$$

(with absorption being negligible).

The temporal profile of the photon density has been obtained from the solution of the diffusion equation[5]:

$$\frac{\partial n(\bar{r}, t)}{\partial t} = D\nabla^2 n(\bar{r}, t) - \frac{v}{l_a} n(\bar{r}, t) + \delta(\bar{r})\delta(t), \quad (3)$$

where the δ function term represents the photon source impulse at time $t = 0$ and position $\bar{r} = 0$. The first term on the right hand side of the equation is the diffusion term, and the second term is the absorption term.

As shown in Figure 1, the early part of the diffuse components is called the snake component that consist of photons that have undergone only a few forward scattering and have traveled along paths slightly deviating from the straight line path. For a weakly absorbing medium, the snake components intensity within a time interval Δt can be written as[15]:

$$I_{snake}(\Delta t) = I_0 A e^{-bL/l_t} = I_0 A e^{-L/l_{snake}}, \quad (4)$$

where A and b are fitting parameters. The exponent b is highly dependent on the time gating interval Δt, and the proportional factor A changes by a factor of 10 as time interval changes from 10 ps to 2000 ps. The snake photon intensity decreases exponentially by a factor of about bL/l_t (eq. (4)), while the ballistic component decreases exponentially by a factor of L/l_s. Since transport length (l_t) is much larger than absorption length (l_s) for tissues the snake component decreases much more slowly than the ballistic component as the tissue thickness increases. One can define a snake scattering length as $l_{snake} = l_t/b$. For $L = 0.5$ mm, $l_t = 2.4$ mm, $l_a = 60$ mm, and $\Delta t = 10$ ps, we obtain $b \sim 0.9$ and $A \sim 1.0 \times 10^{-5}$ for eq. (4). These snake photons play a crucial role in thick tissue imaging where detecting the coherent component is almost impossible.

Several detection schemes have been developed over the years based on frequency domain[1,2,8–10] and time-resolved approaches to sort out ballistic, snake and diffuse photons for imaging in a turbid medium. Time-domain methods based on streak camera[5,13,14], optical Kerr gate[37], electronic time gate[31,32], stimulated Raman amplification[16], cross-correlation second harmonic generation[5,23], heterodyne detection[19], optical coherence tomography[20], upconversion time-gate[29] and holographic method[17,18] have been developed. Keeping the scope of this paper in mind, we briefly describe in the following sections the streak camera, Kerr–Fourier gate and picosecond electronic time-gated optical imaging techniques.

Time-resolved imaging with streak camera

Streak camera is used for direct measurement of the temporal profile of a short pulse with a time resolution as low as 1 ps. Combined with a spectrometer it can be used to yield a temporal and spectral 3D intensity profile of the pulse. The desired signal is first projected onto the camera slit and an optical image is formed on a photo-cathode of the streak tube. Electrons generated in proportion to the incident intensity are accelerated forward and swept by the onset of a high-speed voltage synchronized to the incident light. These electrons then get multiplied in a micro-channel plate and are bombarded against a phosphor screen forming a streak image that gives the temporal intensity profile of the incident pulse. In addition to high time resolution, the camera is sensitive to very low light and can be used for photon counting experiments.

Biomedical imaging requires the ability to discern various tissue types in a complex biological structure like breast or brain. Here we describe how one can probe the difference in the optical properties of different tissues with time-resolved streak camera measurements. By suitably time gating the snake photons one can obtain information that otherwise would not have been possible. Taking advantage of the higher scattering properties of fat tissue, we were able to locate a thin strip of chicken fat inside a thick slab of chicken breast tissue[14].

A schematic diagram of the experimental setup for time-resolved measurements is shown in Figure 2.

Ultrafast 100 fs laser pulses (repetition rate: 82 MHz, λ: 620, beam diameter: 3 mm) of 0.1 nJ per pulse were generated from a colliding pulse mode-locked dye laser system. The main beam was focused into a 0.3 mm spot by a long focal length lens and was allowed to pass through the random scattering medium. Two samples of different dimensions were prepared by embedding a thin strip of chicken fat in the middle of a thick, smooth chicken breast tissue. The samples were prepared by sandwiching the thin strip of fat between the two soft pieces of chicken breast tissues. These samples were pressed between two parallel glass plates to keep them uniformly thick. The first sample had a 2 mm thick, 5 mm wide and 40 mm high fat strip embedded in the middle of a 26 mm thick, 70 mm wide and 40 mm high chicken breast tissue. The sample holder was mounted on a translation stage to let the laser beam scan across the fat strip (Figure 3 *a*). The transmitted signal was detected by a synchroscan streak camera with a 10 ps resolution. Small apertures were used to collect the transmitted photons scattered in the forward direction. These measurements were repeated on a second sample with a 2.5 mm thick, 7 mm wide and 40 mm high strip of fat inside a 40 mm thick, 70 mm wide and 40 mm high chicken breast tissue.

The transport mean free path (l_t) and the absorption length (l_a) for the fat and the chicken breast tissues were obtained from fitting the diffusion equation to the transmitted intensity profiles. The values for fat and chicken breast tissues at 625 nm were measured to be: $l_t = 0.5$ mm, $l_a = 139.3$ mm, and $l_t = 2.5$ mm, $l_a = 51.7$ mm, respectively.

Figure 3 *b* shows two temporal profiles of transmitted pulses propagating through the 26 mm thick tissue: the dotted curve is for the case when the line of beam incidence passes through the center of the fat strip and the solid curve is when the line passes about 5 mm away from the center of the strip. There is a significant difference in the intensities of the early parts of the two transmitted signals while the later portions merge with each other. This difference at the early part is due to much stronger scattering in the fat tissue compared to the chicken breast tissue. Since the absorption length is much larger compared to the transport mean-free path in both tissues, the loss of light due to absorption is negligible compared to the loss due to scattering. This pronounced intensity difference in the early portion of the profile suggests the suitability of snake photons in obtaining the maximum contrast for imaging.

The straight line propagation time through a 26 mm thick tissue is about 116 ps. The time-integrated intensities for four different time windows, 220–820 ps, 120–967 ps, 120–170 ps and 120–130 ps, were calculated from the transmitted signal for various positions of incidence on the sample. The last window captures 10 ps of snake light. The results are plotted in Figure 4. The integrated

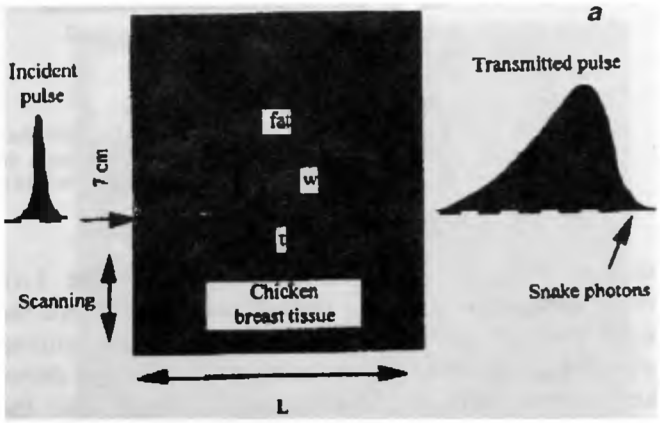

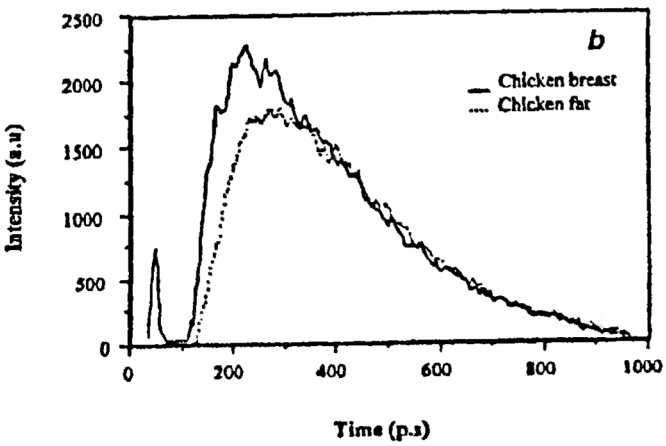

Figure 3. *a*, A cross-section of the chicken breast tissue sample in the plane of the scanning with a thin fat strip embedded in it. The thickness (L) of the breast tissue was 2.6 and 4 cm for the two samples. The thickness (t) for the fat strip was 2 and 2.5 mm and the width (w) was 5 and 7 mm respectively. *b*, Temporal profiles of two transmitted pulses through the 2.6 cm thick sample: the dotted curve is for incidence through the center of the fat strip, while the solid curve is at a 5 mm distance away from the center (after ref. 14).

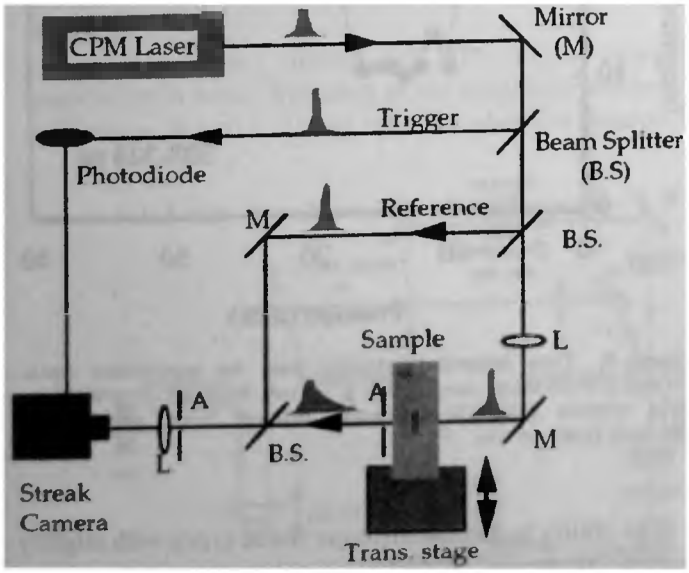

Figure 2. Experimental setup for the detection of snake photons to image translucent objects hidden inside highly scattering random media (after ref. 5).

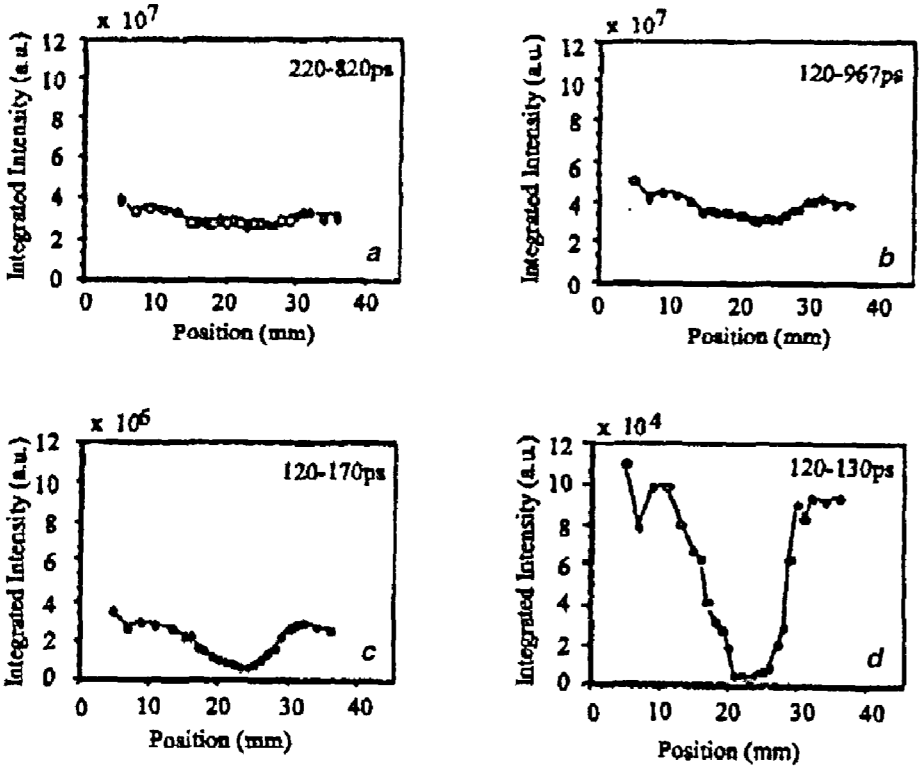

Figure 4. Time integrated intensity from the transmitted signal through a 2.6 cm thick sample at different time gates versus different beam incidence positions. *a*, 220–820 ps; *b*, 120–967 ps; *c*, 120–170 ps; and *d*, 120–130 ps (after ref. 14).

intensity using the 220–820 ps time-gate (Figure 4 *a*), which collects most of the transmitted pulse except the snake photons, shows an almost straight line without revealing the position of the fat tissue. Figure 4 *b* shows the integrated intensity for the whole signal; and the inclusion of the snake photons, though dominated by the late arriving diffuse photons, reveals a very shallow dip around the position of the fat tissue. This case is equivalent to cw transillumination.

The 120–170 ps time-gate, which eliminates a significant portion of the diffused transmitted signal, displays a dip in the integrated intensity curve at the fat region (Figure 4 *c*). The spatial resolution is significantly improved with the 120–130 ps time-gate (Figure 4 *d*) by eliminating the late arriving photons further. By choosing mostly the snake photons (for 10 ps window), not only is the location of the fat tissue correctly predicted, but the edges of the strip are also resolved. The relatively flat bottom of the curve matches well with the width of the fat strip inside the breast tissue with a millimeter resolution.

These measurements were successfully repeated on a 4 cm thick sample with a fat strip inside it. As in the 2.6 cm thick sample, the integrated intensity curve shows a nearly flat line at the region of the fat strip, and it rises sharply once we scan past the edges of the fat strip (Figure 5).

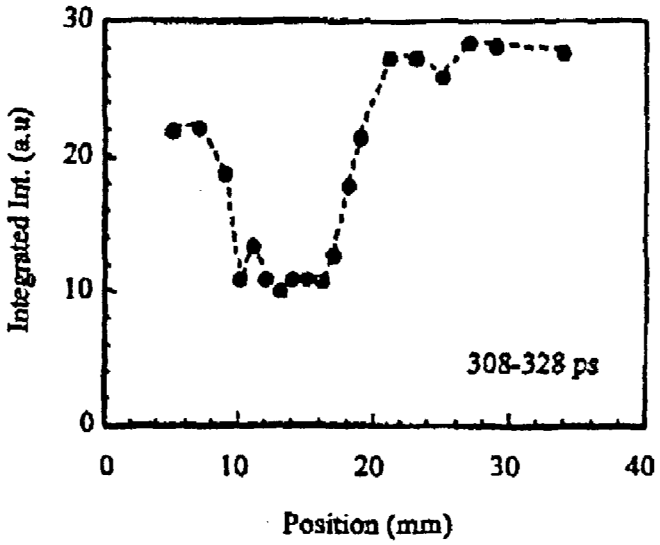

Figure 5. Time integrated intensity from the transmitted signal through a 4 cm thick sample with a 2.5 mm thick fat strip within a 20 ps window (308–328 ps) versus different beam positions of incidence (after ref. 14).

The ability to discern different tissue types with slightly varying scattering properties is a key step in the development of optical mammography and tomography systems. Currently work is in progress to extend this research to two-dimensional breast imaging on human subjects by

using a pair of multi-fiber source and detector bundles with automated data acquisition using a 2 ps synchroscan streak camera. Multi-dimensional images can be reconstructed from these time-resolved intensity profiles by selectively choosing various time slices in inverse reconstruction algorithms.

Time-resolved two-dimensional Kerr–Fourier imaging

Kerr–Fourier imaging uses optical Kerr effect, a third-order nonlinear process, in conjunction with a 4F imaging setup for simultaneous space- and time-gating. In optical Kerr gate an ultrafast shutter is opened when an intense laser pulse induces a transient birefringence in a Kerr active material like carbon disulfide placed between a pair of crossed polarizers, allowing a part of the signal pulse coincident with the triggering pulse in time and space to pass through. A standard 4 F Fourier imaging technique is introduced to this Kerr gate scheme to obtain the Kerr–Fourier gate (KFG) imaging setup as shown in Figure 6.

In our case the KFG was used to image droplets of water and intralipid at various concentrations released into a scattering medium of intralipid suspension in water. A pico-second mode-locked Nd^+: glass laser system provided an 8 ps laser pulse train at 1054 nm to illuminate the sample and its second harmonic at 527 nm was used to trigger the Kerr material, carbon disulfide (CS_2)[37]. Two lenses were introduced into the Kerr cell such that the signal from the sample kept at the front focal plane of the first lens was transformed on to the Kerr cell located at the back focal plane. A second lens was put between the Kerr cell and the CCD camera keeping them at the front and the back focal plane respectively, in order to retransform the Fourier spectrum and image on to the detector.

A two per cent diluted (of 10% stock) intralipid suspension in water was used as the scattering medium in a 50 mm × 50 mm × 50 mm cell. The phantom droplets of

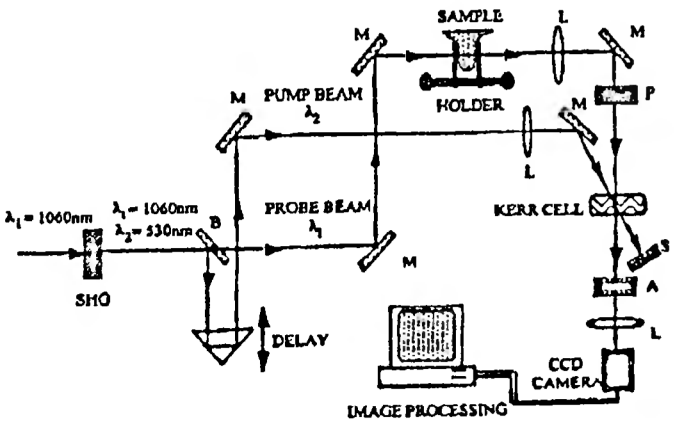

Figure 6. Schematic diagram of a typical Kerr–Fourier imaging setup.

diluted intralipid at various concentrations and pure water were dropped from a controlled burette into the scattering medium and two-dimensional images were recorded. The delay time between the stopper opening and the recording time was between 2 and 10 s. Figure 7 shows two two-dimensional KF images of water droplets emerging from the burette inside the scattering medium. The water droplets were brighter than the host scattering medium as there was less loss of light due to little scattering and absorption in water drops. Similar two-dimensional images of 1, 2, 3 and 5% intralipid droplets were obtained. The image of the 1% droplet was brighter than the host medium due to less scattering and the 2% droplet was almost invisible and the images of the 3 and 5% droplets were darker than the host due to stronger scattering.

The high sensitivity of this Kerr–Fourier scheme marked by its ability to differentiate objects with small differences in scattering properties at a signal level attenuated by a factor of about 10^{-10} from the incident intensity underlines the scope of this ultrafast detection

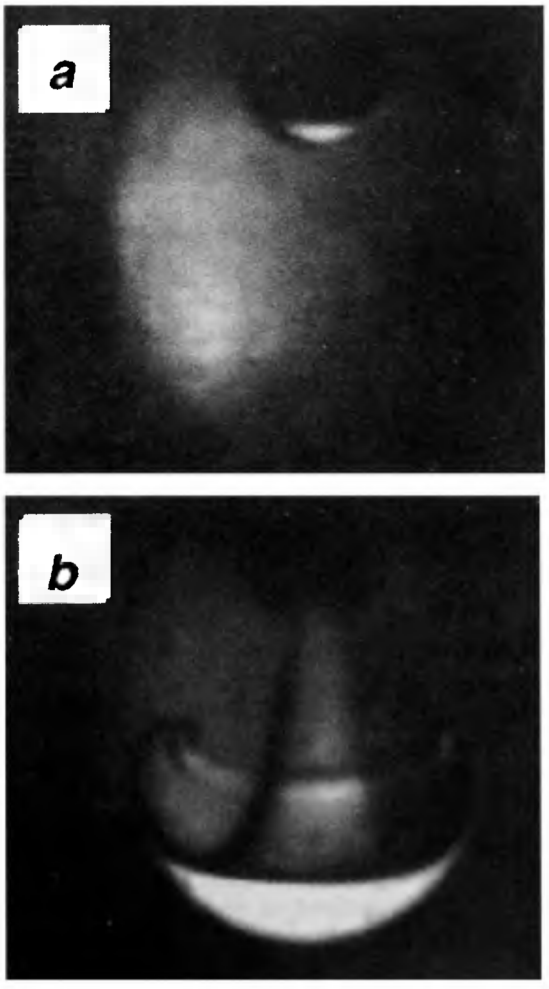

Figure 7. Early time two-dimensional shadow images of a water droplet at a delay of (*a*) 2 s and (*b*) 10 s from the release of the dropper (after ref. 37).

modality in biomedical imaging. The feasibility of reconstructing three-dimensional images from multiple two-dimensional shadowgrams obtained from KFG measurements using a backprojection algorithm has been demonstrated[38].

Two-dimensional electronic time-sliced imaging

This approach uses an electronically controlled time-gate to select the information carrying snake photons to obtain 2-dimensional images directly. Ultrashort laser pulses of about 130 fs duration at 800 nm, at an 82 MHz repetition rate from a self-modelocked Ti : sapphire laser (Spectra Physics Tsunami) were amplified with a regenerative amplifier. The average amplified beam power used in the transillumination imaging experiment was approximately 400 mW at a repetition rate of 1 kHz. The beam was expanded and the central part of it was selected using an aperture to illuminate the sample. This was done in order to make the spatial intensity distribution of the beam smoother and to reduce the intensity difference between the center and the periphery of the beam. Light transmitted through the sample was recorded using an ultrafast electronic-gated imaging camera system (La Vision, Pico-Star) consisting of a time-gated image intensifier unit fiber optically coupled to a charge-coupled device (CCD) camera. The transmitted light from the sample was collected by a camera lens and directed to the image intensifier. The imaging system provided an electronic gate pulse whose full-width-at-half-maximum (FWHM) duration could be adjusted to a minimum of approximately 80 ps, and whose position could be varied in steps of 25 ps over a range of 20 ns. The transillumination signal recorded by the system at a particular gate position was a convolution of the transmitted light pulse with the gate pulse centered on the gate position. The image recorded by the CCD camera was displayed on a personal computer.

Measurements using this electronic time-sliced imaging technique have been performed on several tissue[31], bone and other model biomedical samples[32]. As displayed in Figure 8 *a*, a breast tissue sample consisting of a cancerous piece placed between two normal pieces of 5 mm nominal thickness and lateral dimensions between 8 and 14 mm was prepared. The pieces were compressed between two glass plates to provide uniform thickness and good physical contact between the adjacent pieces of tissue.

Two-dimensional time-sliced transillumination images of this combined breast tissue sample for 0 and 200 ps gate positions are shown in Figure 8 *b*, respectively. The zero position was defined to be the arrival time of the light pulse through a 5 mm thick glass cell filled with water. Figure 8 *c* shows two integrated intensity profiles along a horizontal area covering all three regions of the tissue sample, indicating the spatial distribution of transmitted light intensity.

In both the 0-ps and the 200-ps images, the cancerous and normal regions are visually separated. The spatial intensity distribution of the 0-ps image, displayed by the thick line in Figure 8 *c*, shows a marked dip in the profile, indicating much lower light transmission through the cancerous region. The width of the dip corresponds to the width of the cancerous region. The situation is completely reversed in the second image of Figure 8 *b*. The corresponding spatial intensity profile, shown by a thin line in Figure 8 *c*, exhibits a peak, indicating higher light transmission through the cancerous region.

This difference in the relative light transmission between the normal and the cancerous human breast tissues at 0 and 200 ps can be attributed to the higher scattering of light by the cancerous tissue. Photons transiting through the cancerous region are scattered more

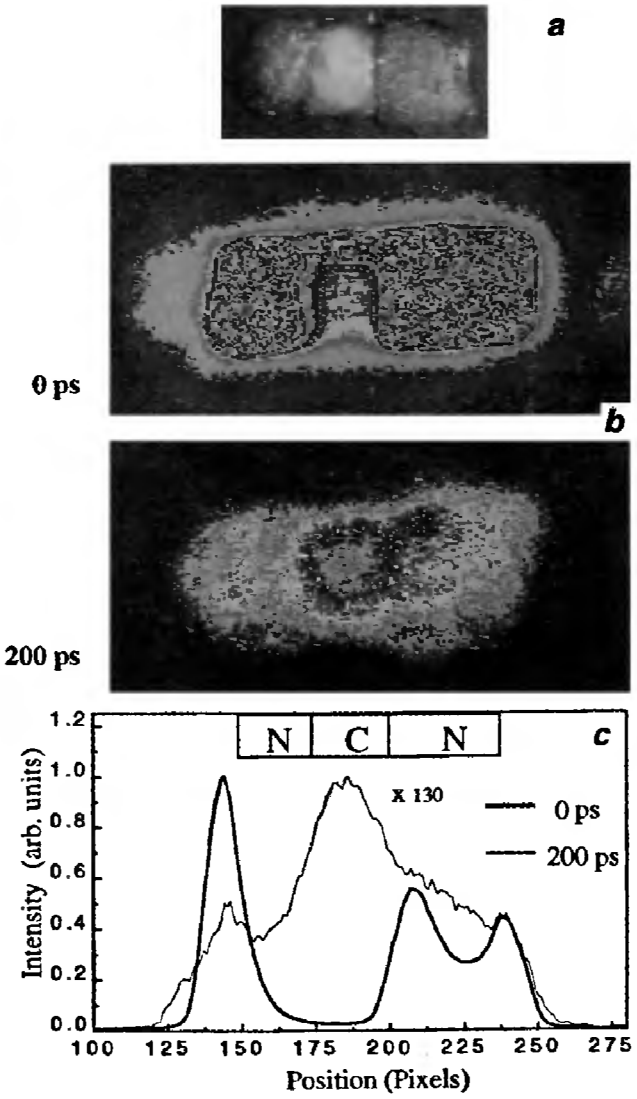

Figure 8. *a*, A photograph of the composite breast tissue sample; *b*, time-sliced transillumination images for gate delays of 0 ps and 200 ps; *c*, normalized spatial intensity profiles of the 0 ps image (thick line) and 200 ps image (thin line) integrated over a horizontal area of 20 pixel vertical width (after ref. 31).

and, consequently, come out later compared to those transiting through the normal region. This results in the intensity profile peak at the cancerous region for the 200 ps image.

In another case, transillumination measurements were performed *in vivo* on a human palm in order to image the metacarpal bones[32]. Figure 9 shows a two-dimensional image of the palm obtained using the time-sliced detection. The 3-cm diameter (approximately) beam was centered on the middle finger as shown in the figure and the time-gate was set at 0 ps to collect the image-bearing photons. The images of the three metacarpal bones (ring, middle and index) are clearly resolved at this time-window. The darker parts show the location of the bones and the lighter parts show the gaps between them. A spatial profile was obtained by integrating the intensity over a 25 pixel wide vertical region that gave a contrast of about 0.66 for the middle finger. The vein going across the region between the middle and the ring fingers appears as the vertical darker part next to the bright central region. Some of the early arriving photons passing through this region are absorbed by the vein resulting in the dark line.

Similar measurements on bones in thick tissues and a small hole in a bone embedded in tissue have also yielded good two-dimensional images[32]. *In vivo* measurement of metacarpal bones yielding high contrast two-dimensional images is highly encouraging to pursue this avenue in development of viable optical alternatives for monitoring bone tumor, bone marrow malignancy, osteoporosis, arthritis, rheumatic disorders and other bone injuries. The ability to obtain two-dimensional images directly in a few seconds of data accumulation is significant from patient's point of view in real-life applications.

Spectroscopic imaging

In a complex tissue structure like breast or brain, a small variation in absorption properties of different tissues can play a significant role in providing key fingerprints in discerning the various tissue-types. Some of the key absorption chromophores in breast tissues are hemoglobin (Hb, HbO_2), water and fat. The absorption characteristics obtained from the transmission measurements on a 3 mm thick human breast tissue[39] is shown in Figure 10.

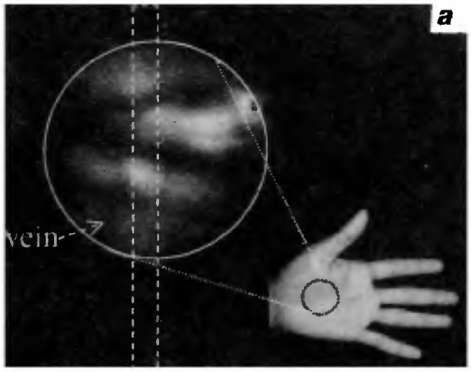

Figure 9. Two-dimensional image of the metacarpal bones of a human palm (after ref. 32).

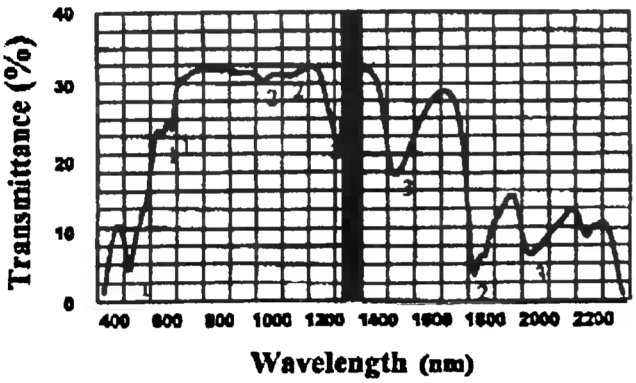

Figure 10. Attenuation spectrum through a 3 mm thick human breast specimen showing the contribution from oxy-hemoglobin (1), fat (2) and water (3) (after ref. 39).

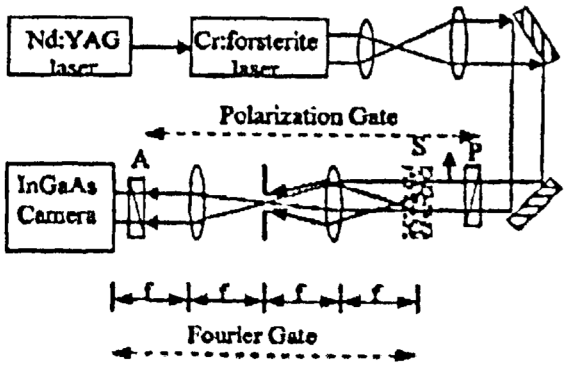

Figure 11. Schematic diagram of the experimental arrangement for two-dimensional NIR spectroscopic imaging.

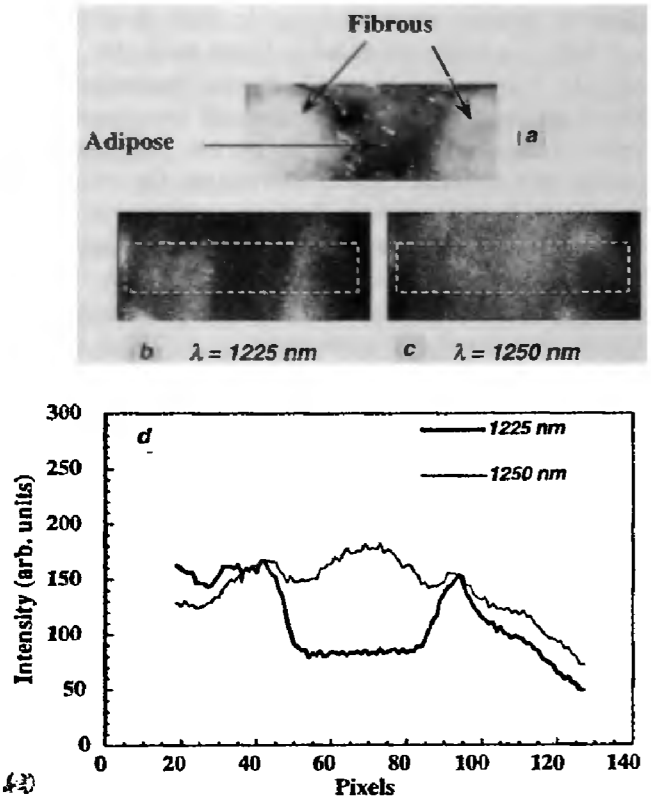

Figure 12. *a*, Black and white photograph of the fatty tissue specimen used in the spectroscopic imaging; *b*, *c*, the transillumination images at 1225 nm and 1250 nm respectively; *d*, corresponding intensity profiles integrated over the region marked by white dashed lines (after ref. 26).

It has been shown by setting the probe wavelengths to absorption bands of tissue components, one can obtain two-dimensional transillumination images with marked distinction between fatty and fibrous human breast tissues[26,31]. This spectral measurement was a part of an investigation to study the effectiveness of using Fourier space-gate and polarization-gate in two-dimensional near-infrared transillumination imaging.

The experimental setup for this experiment is displayed schematically in Figure 11. A Cr^{4+} : forsterite laser pumped by a Nd : YAG laser provided 1225 nm and 1250 nm light for transilluminating a section of 35 mm × 14 mm × 5 mm human breast tissue. The specimen had a section of fatty tissue with fibrous tissue on two sides (Figure 12 *a*). The 1225 nm wavelength falls in the absorption band of fat while 1250 nm is completely nonresonant with it. Two-dimensional transillumination images of this sample at 1225 nm and 1250 nm are shown in Figure 12 *b* and *c*. The fatty region is darker and clearly distinguished from the fibrous regions on the two sides in the 1225-nm image as it is tuned to the absorption band. On the other hand, the 1250 nm-image shows no appreciable difference between the regions. Two spatial intensity profiles integrated over the areas highlighted by white dashed lines in the corresponding images are displayed in Figure 12 *d*. Because of the absorption due to fat, the intensity profile for the 1225-nm image shows a distinct dip in the fat region. No such dip is observed in the other profile. This result shows that spectroscopic differences can be used to obtain high contrast optical images of tissues by tuning to suitable wavelengths. This spectral technique can be used in conjunction with other time-resolved measurements to improve image quality.

Conclusion

Ultrafast photonic methods based on various time-gating approaches have opened up new avenues in non-invasive optical imaging. We have briefly reviewed some of the currently pursued time-domain methods. The ability to obtain physiological information from spectroscopic fingerprints of the molecular constituents of tissue like water, fat, oxy- and deoxyhemoglobin by carefully selecting wavelengths in the visible and near-infrared region makes these optical approaches more promising than X-rays and other imaging modalities.

Non-invasive and non-ionizing spectroscopic optical tomography systems based on time-resolved modalities are on the horizon.

1. Tuchin, V. V., *Selected Papers on Tissue Optics: Applications in Medical Diagnostics and Therapy*, SPIE Milestone Series, 1994, MS102.
2. Muller, G. *et al.* (eds), *Medical Optical Tomography*, 1993, SPIE, **IS11**, Birmingham.
3. Chance, B., *Annu. Rev. Biophys. Biophys. Chem.*, 1991, **20**, 1–28.
4. Gayen, S. K. and Alfano, R. R., *Opt. Phot. News*, 1996, **7**, 17–22.
5. Das, B. B., Liu, F. and Alfano, R. R., *Rep. Prog. Phys.*, 1997, **60**, 227–292.
6. Hebden, J. C., Arridge, S. R. and Delpy, D. T., *Phys. Med. Biol.*, 1997, **42**, 825–840.
7. Arridge, S. R. and Hebden, J. C., *Phys. Med. Biol.*, 1997, **42**, 841–853.
8. Lakowicz, J. R. and Berndt, K., *Chem. Phys. Lett.*, 1990, **166**, 246–252.
9. Svaasand, L. O., Tromberg, B. J., Haskell, R. C., Tsay, T. -T. and Burns, M. W., *Opt. Engg.*, 1993, **32**, 258–266.
10. French, T., Gratton, E., Maier, J., *Proc. SPIE*, 1992, **1640**, 254–261.
11. Ferrari, M., De Blasi, R. A., Safoue, F., Wei, Q. and Zaccanti, G., *Optical Function of Brain Function and Metabolism*, Plenum, New York, 1993, pp. 21–31.
12. Anderson-Engels, S., Berg, R., Svanberg, S. and Jarlman, O., *Opt. Lett.*, 1990, **15**, 1179–1181.
13. Hebden, J. C., Kruger, R. A. and Wong, K. S., *Appl. Opt.*, 1991, **30**, 788–794.
14. Das, B. B., Yoo, K. M. and Alfano, R. R., *Opt. Lett.*, 1993, **18**, 1092–1094.
15. Liu, F., Yoo, K. M. and Alfano, R. R., *Opt. Lett.*, 1993, **19**, 740–742.
16. Reintjes, J., Duncan, M., Bashkansky, M., Moon, J., Mahon, R., Tankersley, L. and Prewitt, J., OSA Proceedings on Advances in Optical Imaging and Photon Migration (ed. Alfano, R. R.), 1994, vol. 21, pp. 129–133.
17. Spears, K. G., Serafin, J., Abramson, N. H., Zhu, X. and Bjelkhagen, H., *IEEE Trans. Biomed. Eng.*, 1989, **36**, 1210–1221.

18. Leith, E., Arons, E., Chen, H., Chen, Y., Dilworth, D., Lopez, J., Shih, M., Sun, P. C. and Vossler, G., *Opt. Photon. News*, 1993, **4**, 19–23.
19. Toida, M., Ivhimura, T. and Inaba, H., *IEICE Trans.*, 1991, **E74**, 1692–1694.
20. Brezinski, M. E., Tearney, G. J., Boppart, S. A., Bouma, B. and Fujimoto, J. G., *Advances in Optical Imaging and Photon Migration*, OSA, 1996, pp. 21–23.
21. Demos, S. G. and Alfano, R. R., *Appl. Opt.*, 1997, **36**, 150–155.
22. de Boer, J. F., Milner, T. E., van Gemert, M. J. C. and Nelson, J. S., *Opt. Lett.*, 1997, **22**, 934–936.
23. Guo, Y., Ho, P. P., Savage, H., Harris, D., Sacks, P., Schantz, S., Liu, F., Zhadin, N. and Alfano, R. R., *Opt. Lett.*, 1997, **22**, 1323–1325.
24. Denk, W., *J. Biomed. Opt.*, 1996, **1**, 296–304.
25. Guo, Y., Wang, Q. Z., Zhadin, N., Liu, F., Demos, S. G., Calistru, D., Turksliunas, A., Katz, A., Budansky, Y., Ho, P. P. and Alfano, R. R., *Appl. Opt.*, 1997, **36**, 968–970.
26. Gayen, S. K., Zevallos, M. E., Alrubaiee, M., Evans, J. M. and Alfano, R. R., *Appl. Opt.*, 1998, **37**, 5327–5336.
27. Devaraj, B., Takeda, M., Kobayashi, M., Usha, M., Chan, K. P., Watanabe, Y., Yuasa, T., Akatsuka, T., Yamada, M. and Inaba, H., *Appl. Phys. Lett.*, 1996, **69**, 3671–3673.
28. Wist, A. W., Moon, P., Meiksin, S., Herr, S. L. and Fatouros, P. P., *J. Clin. Laser Med. Surg.*, 1993, **11**, 313–321.
29. Farris, G. W. and Banks, M., OSA Proceedings on Advances in Optical Imaging and Photon Migration (ed. Alfano, R. R.), 1994, vol. 21, pp. 139–142.
30. Prapavat, V., Schutz, R., Runge, W., Beuthan, J. and Muller, G., *Proc. SPIE*, 1995, **2626**, 121–129.
31. Gayen, S. K., Zevallos, M. E., Das, B. B. and Alfano, R. R., *Adv. Opt. Imaging Photon Migration*, 1998, **21**, 63–66.
32. Zevallos, M. E., Gayen, S. K., Das, B. B., Alrubaiee, M. and Alfano, R. R., in *J. Sel. Topics Quant. Electr. Lasers Med. Biol.*, (to be published).
33. Ishimaru, A., *Wave Propagation and Scattering in Random Media*, Academic, New York, 1978.
34. Ishimaru, A., *Appl. Opt.*, 1989, **28**, 2210–2215.
35. Wang, L., Ho, P. P., Liu, C., Zhang, G. and Alfano, R. R., *Science*, 1991, **253**, 769–771.
36. Chandrasekhar, S., *Radiative Transfer*, Oxford University Press, London, 1950.
37. Alfano, R. R., Liang, X., Wang, L. and Ho, P. P., *Science*, 1994, **264**, 1913–1915.
38. Kalpaxis, L. *et al.*, *Opt. Lett.*, 1993, **18**, 1691–1693.
39. Marks, F. A., *Proc. SPIE*, 1992, **1641**, 227–237.

ACKNOWLEDGEMENTS. We thank our co-workers S. K. Gayen, M. E. Zevallos, P. P. Ho, F. Liu, K. M. Yoo, L. Wang, X. Liang, J. M. Evans, and M. Alrubaiee for their contribution to these research projects. This work was supported by the New York State Science and Technology Foundation, NAA IRA Program, DOE through the Center of Excellence Program, the Heat program of the City University of New York.

MEETINGS/SYMPOSIA/SEMINARS

National Symposium on 'Microbials in Insect Pest Management'

Date: 24–25 February 2000
Place: Chennai, India

The symposium envisages the recognition of the value and use of microbials for insect pest management. The topics include: Identification and development (including molecular) of new microbial agents for pest control; Microbial testing against plant pathogens; Microbes in plant defense aid; Chemistry of plant–microbe interaction; Mass production and utilization; and Microbial management (education, manpower development and economics).

Contact: Dr S. Ignacimuthu
Entomology Research Institute
Loyola College
Chennai 600 034, India
Telefax: 91-44-8265542
E-mail: erilc@tn.nic.in

International Conference on Polymer Characterization (POLYCHAR 8)

Date: 11–14 January 2000
Place: University of North Texas, USA

Themes include: Predictive methods; Polymerization; Polymer liquid crystals; Mechanical properties and performance; Dielectric and electrical properties; Interfaces; Rheology and Processing.

Contact: Prof. R. P. Singh
Scientific Committee Member from India
Materials Science Centre
Indian Institute of Technology
Kharagpur 721 302, India
Tel: (O) 91-3222-83982
(R) 91-3222-83983
Fax: 91-3222-55303
E-mail: rps@matsc.iitkgp.ernet.in

International Commemorative Symposium: 70th Anniversary of the Japanese Society of Fisheries Science

Date: 1–5 October 2001
Place: Yokohama, Japan

Themes include: Roles and contribution of fisheries and marine sciences in the 21st century; Fisheries biology and management; Aquatic environment and its conservation; Aquaculture; Aquatic biology and genetics; Post-harvest: Science & Technology; Fishery economics and distribution; Fisheries engineering; International cooperation activities; Education system in fisheries and marine science.

Contact: Dr Toshiaki Ohshima
Tokyo University of Fisheries
Konan 4-5-7, Minato
Tokyo 108-8477, Japan
Tel: 81-3-5463-0613
Fax: 81-3-5463-0627
E-mail: symp70yr@tokyo-u-fish.ac.jp